Electrochimica Acta 476 (2024) 143707

Contents lists available at ScienceDirect

Electrochimica Acta

journal homepage: www.journals.elsevier.com/electrochimica-acta

Using ultrasound to increase copper and nickel dissolution and prevent passivation using concentrated ionic fluid.

Christopher E. Elgar [a,*], Sam Ravenhill [a], Philip Hunt [a], Ben Jacobson [b], Andrew Feeney [b], Paul Prentice [b], Karl S. Ryder [a], Andrew P. Abbott [a]

[a] School of Chemistry, University of Leicester, LE1 7RH, Leicester, United Kingdom
[b] James Watt School of Engineering, University of Glasgow, G12 8QQ, United Kingdom

ARTICLE INFO

Keywords:
Sonication
Anodic dissolution
Deep eutectic solvents
Ultrasound

ABSTRACT

This paper uses targeted ultrasound on a surface undergoing anodic dissolution. The aim of these experiments was to etch metals that would normally passivate. The study was carried out in deep eutectic solvents (DESs) as these are technologically useful for metal processing but suffer the disadvantages of being viscous and hence have slow mass transport which results in metal passivation. Linear sweep voltammetry showed a linear current-voltage response at potentials anodic (more positive) of the oxidation potential under sonication. Passivation was observed in silent conditions. It was also shown that the dissolution current was roughly 14 times larger under sonication. High speed imaging showed asymmetric bubble collapse leading to enhanced removal of material from the surface with etch rates as high as 3.8 μm.min^{-1} under ultrasonic conditions.

1. Introduction

The electrodeposition and dissolution of metals is usually diffusion limited and this controls dissolution rates and surface morphology. The electrolyte can also result in the passivation of some metals where mass transport is slow. The rate of mass transport to the electrode surface can be increased using forced convection such as jets, rotating discs or ultrasound. Previous work to increase mass transport has involved the use of different techniques that increase the movement of the electrolyte around the electrode area. For example, with a rotating disc electrode (RDE), the rotating working electrode introduces a localised flux to the electrolyte, allowing for a greater mixing of species and removal of insoluble passivating layers [1]. The speed of rotation allows for control of the electrolyte flux, and thus offers a degree of current control [2]. While the RDE is a form of localised stirring, laminar and turbulent flow can also be employed as a methodology to increase mass transport at an electrode surface [3].

Electrochemical modification using jets has been carried out for both electrodeposition and micromachining [4,5]. Using electrolyte jet speeds in the region of 20 m.s^{-1} and 200 mL.min^{-1}, current densities of typically 200 A.cm^{-2} can be applied. This leads to rapid localised etching of surfaces which are useful for dynamic micromachining.

Ultrasonics can be used to introduce forced convection into electrochemical reactions, via three main mechanisms: cavitation collapse, microjets, and acoustic streaming [6]. Cavitation occurs from the rapid oscillation of the ultrasonic device, causing low- and high-pressure waves to propagate through the solution which allow bubbles to form. The continued oscillation causes expansion and shrinking of the bubbles until they reach a critical size and collapse, sending out shock waves through the solution. If the cavitation is located close to a solid surface, such as an electrode, the collapse occurs asymmetrically causing powerful microjets to bombard the surface. The energy release of asymmetric collapse can be considerable, but will depend upon the solvent, applied ultrasonic frequency, ultrasonic intensity, and temperature of the solution [7,8]. The acoustic streaming effect causes a mixing of the bulk electrolyte, leading to a thinning of the diffusion layer at the electrode surface [9] compared to the silent conditions, with a dependency on the applied ultrasonic power level [10] as well as the separation distance of the electrode and horn [11].

Most forced convection studies have focussed on electrodeposition due to its importance is electroplating [12] but electrodissolution is also important for electropolishing and electrorefining. Most electrochemical deposition and dissolution of metals has been carried out in aqueous solutions but an increasing body of work uses ionic liquids and deep eutectic solvents due to their ability to tune speciation and redox properties [13]. It has been shown that the high viscosity of these

* Corresponding author.
E-mail address: cee17@leicester.ac.uk (C.E. Elgar).

https://doi.org/10.1016/j.electacta.2023.143707
Received 10 November 2023; Received in revised form 15 December 2023; Accepted 21 December 2023
Available online 22 December 2023

concentrated ionic media limits the rates of all electrochemical processes [14]. The electrodissolution of 9 metals in DESs was shown to result in passive film formation [15]. Little work has been carried out using ultrasonication in DESs, except for a preliminary study of the insonated electrodeposition of copper in choline chloride (ChCl) and 2 molar equivalents of glycerol which showed a roughly 200 times increase in the deposition rate compared to silent conditions [16].

The aim of this study is to carry out electrodissolution of copper and nickel in a deep eutectic solvent formed from ChCl and ethylene glycol (EG), and show that when ultrasound is applied directly to the surface of an electrode there is a significant increase in the dissolution current due to the lack of electrode passivation.

2. Material and methods

All chemicals were used as supplied, without further purification. The DES solution was prepared from 1 mol eq. of choline chloride (Sigma Aldrich, > 98%) and 2 mol eq. of ethylene glycol (Fisher Scientific, 98 %). The solvent was prepared by stirring the components at 60 °C until a colourless homogeneous liquid was formed. The solvent was removed from the heat and stored at room temperature in sealed storage bottles. To limit the effects of variations in water content, the same batch of ChCl:2EG was used throughout this work.

Anodic linear sweep voltammetry (LSV) experiments were performed at 20 °C, using a Metrohm Autolab PGStat302N potentiostat, together with the corresponding Nova 2.1 software. A 3-electrode set-up was used, consisting of a 1.25 mm diameter hooked Cu- disc or Ni-disc working electrode, a copper or nickel wire reference electrode (corresponding to the working electrode), and an IrO_2 coated Ti mesh as counter electrode. The LSV curves were recorded at scan rates between 10 and 100 $mV.s^{-1}$. Prior to use, electrodes were polished on 800 grit, 1200 grit, and finally 3200 grit sandpaper. For the LSV experiments with ultrasound, a 20 kHz commercial ultrasonic system from Fisherbrand was used, connected to a CL-334 ultrasonic probe (diameter: 13 mm) operating with power variable up to 700 W (527 $W.cm^{-2}$). Chronoamperometry experiments were performed at 20 °C, using a 3-electrode set up consisting of a metal plate (copper or nickel) masked with stopping-off lacquer number 45 (MacDermid Enthone), leaving an exposed area of roughly 1 cm^2 as the working electrode, a copper or nickel wire reference electrode, and an IrO_2 coated Ti mesh as the counter electrode.

For these experiments, the ultrasonic horn was placed at a distance of 4 mm above the working electrode. The experiments were carried out in 200 mL of solvent at 20 °C. Ultrasound was applied during the whole period that the anodic scan lasted.

3D optical images of the sample were captured by using a Zeta Instruments Zeta 2000 optical profiler using the inbuilt Zeta3D software version 1.8.5. Images were constructed by determining the features of an image that are in focus at different heights, resulting in a 3D topographical map of the surface. Areas were calculated from the 2D images of the complete unmasked areas using ImageJ software version 1.5.1 [17].

The cavitation activity and mass transport effects induced within the DES by the ultrasound was assessed via high-speed imaging (Fastcam SA-Z 2100 K, Photron, Bucks UK). The ultrasonic source used was a 500 W, 20 kHz ultrasonic horn (Sonics, Newton, Connecticut USA), with data collected over 1 s sonications at 40% input power (707 $W.cm^{-2}$). The electrode surface was positioned ca. 4 mm below the tip of the ultrasonic horn with imaging sequences captured at 80,000 frames per second (fps) via a macro lens (Milvus 100 mm f/2 M, Zeiss, Oberkocken Germany) achieving a spatial resolution of 26 $\mu m.pixel^{-1}$. Illumination was provided via synchronous 10 ns laser pulses at 640 nm (CAVILUX Smart, Cavitar, Tampere Finland), coupled to a liquid light guide and a collimating lens. This configuration facilitates shadowgraphic imaging, whereby refractive index variations introduced through density and pressure fluctuations during the sonication, are also apparent [18,19]. The spatial and temporal resolution is optimal for capturing the cavitation dynamics and mass transport effects throughout the sonication.

3. Results and discussion

3.1. Linear sweep voltammetry (LSV)

The electro-dissolution of two metals, copper and nickel, has been investigated in ChCl:2EG under silent and ultrasonic conditions using a fixed electrode–ultrasonic horn distance, with varying intensities from the horn. Measurements were referenced to the corresponding metal wire in solution to allow a direct comparison of the effect of overpotential on the different systems.

Fig. 1a and 1b show the LSV curves for copper and nickel in ChCl:2EG respectively. Under silent conditions, the copper surface undergoes a sudden drop off in current, suggesting a passivation process due to the formation of poorly soluble copper species, such as CuCl, [15] while nickel oxidation shows a slower formation of a passivating layer, likely from the formation of mixed nickel species, e.g. $[NiCl_4]^{2-}$, NiO, $Ni(OH)_2$, and $Ni(OC_2H_4OH)_2$, before dropping off completely, suggesting the formation of a possible porous layer first, followed by the formation of a more solid non-conductive layer [20].

Under the effects of ultrasound, the LSV curves do not show a decrease in current from passivation of the electrode surface. The current density for copper dissolution at an overpotential of 1.4 V has risen from ca. 20 $mA.cm^{-2}$, to 270 $mA.cm^{-2}$, a 14 times increase in current density. The current density for nickel dissolution rises from ca. 10 $mA.cm^{-2}$ under silent conditions, to about 300 $mA.cm^{-2}$ under ultrasonic conditions.

Ultrasound provides a clear increase in mass transport to and from the electrode surface, reducing the surface concentration and ensuring the layer close to the electrode does not become super-saturated with metal ions.

The current-voltage response is somewhat unusual as there is an approximately linear correlation. This could be due to forced convection or migration rather than diffusion, although the former is unlikely as copper and nickel dissolution have been studied using rotating disc and flow electrodes and both have shown diffusion limited processes[21]. The current for Cu oxidation in the LSV curve decreases with increasing sweep rate when the electrode is sonicated. Under silent conditions, the current for copper oxidation increases with increasing sweep rate as expected. (Fig. 2)

This shows that the current is limited by the conductivity of the solution close to the electrode surface. It is probable that the very high copper dissolution rates increase the amount of metal ions close to the electrode surface and increase the local conductivity. This would account for the increase in current with decreasing potential sweep rate.

A method to confirm this explanation of the non-diffusional response to LSV curves would be to repeat the experiments using media of known viscosity and conductivity (Table S1). It has recently been shown that ChCl–water mixtures behave in a similar manner to DESs once the ChCl concentration is greater than 1 $mol.kg^{-1}$ [22]. Fig. 3 shows the slopes of insonated LSV curves measured in ChCl:2EG, ChCl:$3H_2O$, ChCl:$4H_2O$, ChCl:$10H_2O$, and ChCl:$50H_2O$ vs the solution conductivity. A linear correlation is observed between the LSV curve slope and the solution conductivity, suggesting the idea that migration is an important component in governing the voltammetric current, possibly limited by the migration of chloride ions to the electrode surface. Fig. 3 also shows that the slope of the linear sweep voltammograms is relatively independent of the power supplied to the ultrasonic horn, confirming that migration is a novel and hitherto unconsidered factor in this type of process.

If diffusion was an element in the dissolution of copper it would be expected that the current would decrease as a function of time in a chronoamperometric experiment. Fig. 4 shows that not only does the current not decrease, it does in fact increase with time. The most

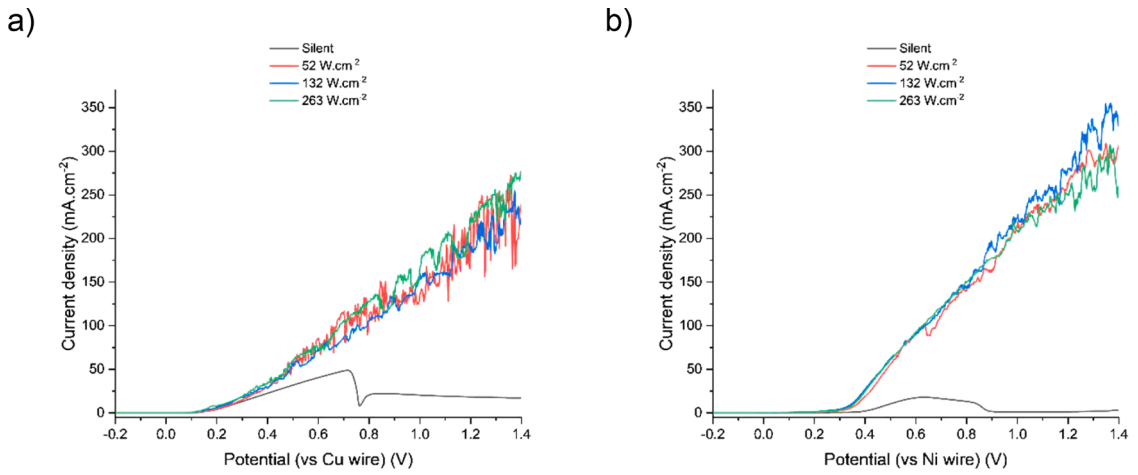

Fig. 1. LSV curves of a) copper, and b) nickel electrodes in ChCl:2EG under silent and ultrasonic conditions. The scan rate was 30 mV.s^{-1} and the reference electrode was a wire of the same metal investigated.

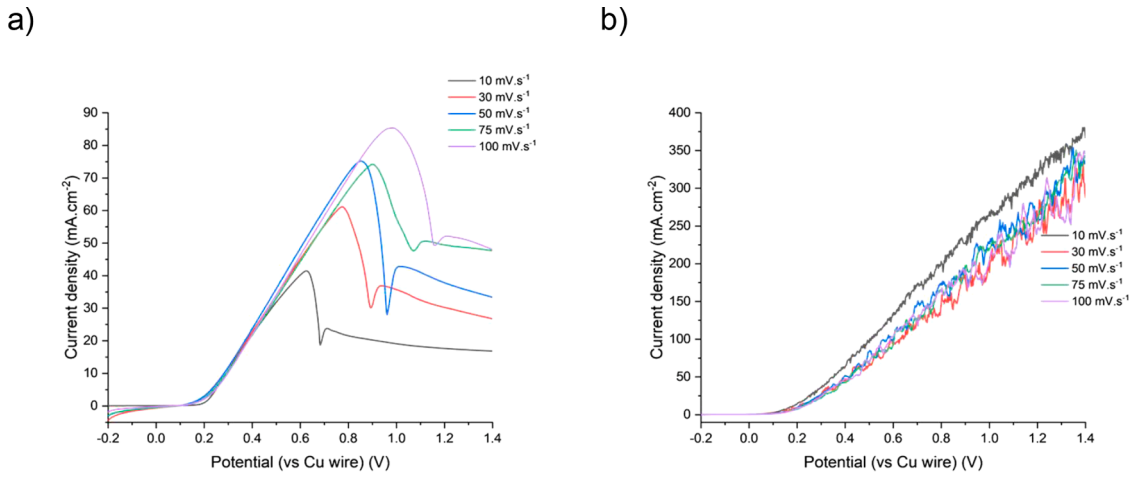

Fig. 2. LSV curves of copper a electrode run under a) silent, and b) insonated (52 W.cm^{-2}) conditions in ChCl: 2EG. The scan rate was 30 mV.s^{-1} and the reference electrode was a copper wire.

probable explanation for this is the rapid increase in surface area as the sample etches (see Fig. 6). This can also be concluded from a comparison of the optical images of copper and nickel (Figs. 6 and 8). It can therefore be concluded that the unusual voltage-current response which arises when voltammetric experiments are carried out using direct sonication results from rapid dissolution, resulting in increased local conductivity and an increase in electrode surface area.

It was previously proposed that during dissolution, the slow diffusion of halide anions to the electrode surface results in oxidised metal ions forming complexes with an incomplete solvation sheath e.g.

$$Cu(I) + Cl^- \rightarrow CuCl$$

This species has limited solubility and has been observed as a solid green deposit on the electrode surface under silent dissolution experiments. [15]

There are no signs of solid deposits in the liquid when ultrasound is used, presumably because enhanced mass transport enables a complete solvation sheath to form.

$$Cu(I) + 2Cl^- \rightarrow [CuCl_2]^-$$

$$Cu(I) + 3Cl^- \rightarrow [CuCl_3]^{2-}$$

$$Cu(II) + 4Cl^- \rightarrow [CuCl_4]^{2-}$$

These species are known to have a high solubility in the DES[23] and the colour of the solution matched with the speciation determined using UV–vis spectroscopy and EXAFS [20].

Moreover, under ultrasound the onset potential of nickel anodic dissolution occurs at progressively lower over-potentials as the ultrasonic intensity increases, i.e. 370 mV in silent conditions to 290 mV under ultrasound. This could be caused by the microjetting from cavitation on the surface removing or weakening the nickel oxide passivation layer [24].

Insonated LSV curves for both metals show spikes in the LSV current. Ultrafast voltammetry and amperometry has shown that spikes in current density are down to cavitation events happening at the surface of the electrode [25–28]. As ultrasonic intensity increases past 263 W.cm^{-2}, the noise decreases significantly due to the acoustic streaming effects becoming more prominent at higher powers, as seen in figures S3 and S4.

3.2. *High speed imaging*

High-speed imaging was used to assess the cavitation activity during the sonication. Fig. 5 presents frames extracted from a 1 s sonication, showing specific cavitation activity and development of acoustic streaming during the sonication.

The sonication initiation is followed by a downwards stream of

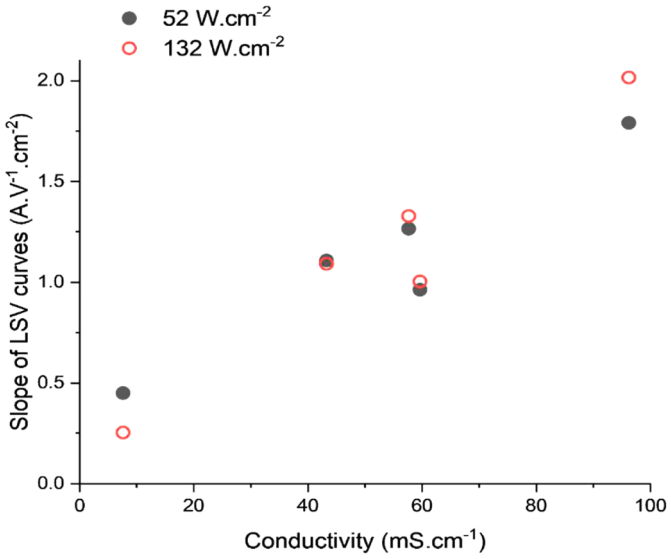

Fig. 3. Slope of sonicated LSV curves recorded in ChCl:2EG, ChCl:3H_2O, ChCl:4H_2O, ChCl:10H_2O, and ChCl:50H_2O vs the solution conductivity. All LSV curves were recorded on a copper disc electrode (1.25 mm diameter) at 30 mV. s^{-1} between −0.5 V and 1.0 V vs $Ag/Ag^{+}_{(aq)}$. Individual LSV curves are available in figure S1 (52 $W.cm^{-2}$) and S2 (132 $W.cm^{-2}$).

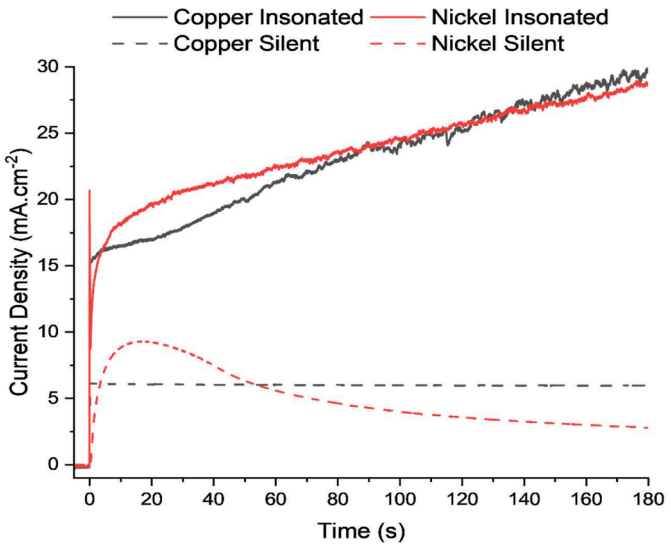

Fig. 4. Sonicated (132 $W.cm^{-2}$) and silent chronoamperometry profiles for copper and nickel run in ChCl:2EG at an applied overpotential of +1.0 V.

bubbles from the centre of the ultrasonic horn tip. This bubble cloud collides with the electrode surface and forms a densely packed bubbly vortex (observed at 12.66 ms), with corresponding acoustic streaming forcing fluid down and outwards from the centre of the electrode [29, 30]. Beyond this, a large bubble cluster, approximately 3 mm wide, is observed in Fig. 5 at 25.98 ms. This primary bubble cluster is generated and sustained by coalescence of multiple bubble clouds and oscillates strongly close to the horn tip. Smaller sub-clusters of varying sizes can be observed throughout the sonication across the cavitation region between the horn tip and electrode. The addition of microstreaming (fluid circulation in the vicinity of bubbles, generating turbulence and improving mixing [30]) from bubble clouds facilitates sustained flow away from the electrode surface which results in increased mass transport throughout the sonication. Additional cavitation-related phenomena such as bubble collapse shockwaves and jetting further enhance the process and are believed to be the source of current density spikes in the LSV curves [31]. Bubble-collapse shockwaves, originating from violently collapsing bubble clouds near the ultrasonic horn tip (arrowed yellow, Fig. 5) were previously reported as important for material delamination [32]. Jetting, which occurs when a bubble deflates and collapses asymmetrically in proximity to a rigid surface, is observed (inset, at 28.01 ms) from single bubbles within a millimetre of the electrode layer[33]. In the example highlighted, the non-spherical bubble has involuted from the bulk-DES side, indicative of a thin column of liquid that rapidly traverses the gas phase, to impact the electrode surface. This jetting has previously been shown to cause micron-sized surface erosion, or pitting, and removal of passivating layers[34,35] as well as being key for metal delamination from printed circuit boards[36] and is believed to be the source of the pitting observed on the electrode surface (Section 3.3).

As the sonication develops, the bubble cloud continues to expand, with a greater density of smaller bubbles occupying the region between the ultrasonic horn and the electrode. This cloud is sustained, with smaller bubble sub-clusters directly impacting the electrode surface throughout the sonication.

3.3. Electrode surface – copper

Fig. 6 shows the morphology of a copper electrode surface before and after LSV scans and marked differences can be seen between silent and insonated conditions. Under silent conditions, the build-up of insoluble copper species has levelled out the surface defects left from polishing. Around the edges, the beginnings of anisotropic etching around the grain boundary can be seen. Contrasting to the insonated surface, grain boundaries are evident across the whole surface from an anisotropic removal of copper brought about by the increase in mass transport from the ultrasonication.

Additionally, bulk copper removal can be seen around the edge of the sonicated electrode (Fig. 6d). The 3D topography of these circular and semi-circular defects shows a depth of ca. 40 μm from the level of the bulk copper, and a diameter of around 60 μm, which can be attributed to the asymmetrical collapse of cavitation bubbles at the surface, resulting in jetting as discussed previously. It should be noted that the time that the copper electrode spends in the dissolution regime is approximately 140 s, indicating that under sonication the metal dissolution is extremely rapid compared to silent conditions.

Bulk electrolysis of a copper electrode (masked copper plate with a 1 cm^2 unmasked circular area at an over-potential of +1.0 V vs copper wire reference for 180 s) showed an etch rate of 3.8 $\mu m.min^{-1}$ could be obtained compared to 0.8 $\mu m.min^{-1}$ under silent conditions (Fig. 7). Repeating the experiment without an applied potential, but with ultrasound, resulted in no change in the surface morphology. The etch rates correlate well with the current densities shown in Fig. 1 and suggest a current efficiency of >90% under sonicated conditions.

3.4. Electrode surface – Nickel

Fig. 8 shows the morphology of a nickel electrode surface before and after LSV scans and again marked differences can be seen between silent and insonated conditions. The surface profile of the nickel electrode shows little change, with only a negligible etch rate under silent conditions. Nickel is a harder metal than copper and so cannot be eroded as easily by cavitation. It is clear that some of the surface roughness, resulting from the electrode pre-treatment, has been removed, but the polishing of nickel under silent conditions has already been demonstrated although over a vastly different timescale and via a totally different mechanism [37]. There were no signs of bulk anisotropy during this time frame, showing that the dissolution mechanism is probably different to that for copper.

Under bulk electrolysis conditions (masked nickel plate with a 1 cm^2 unmasked circular area at an over-potential of +1 V vs nickel wire

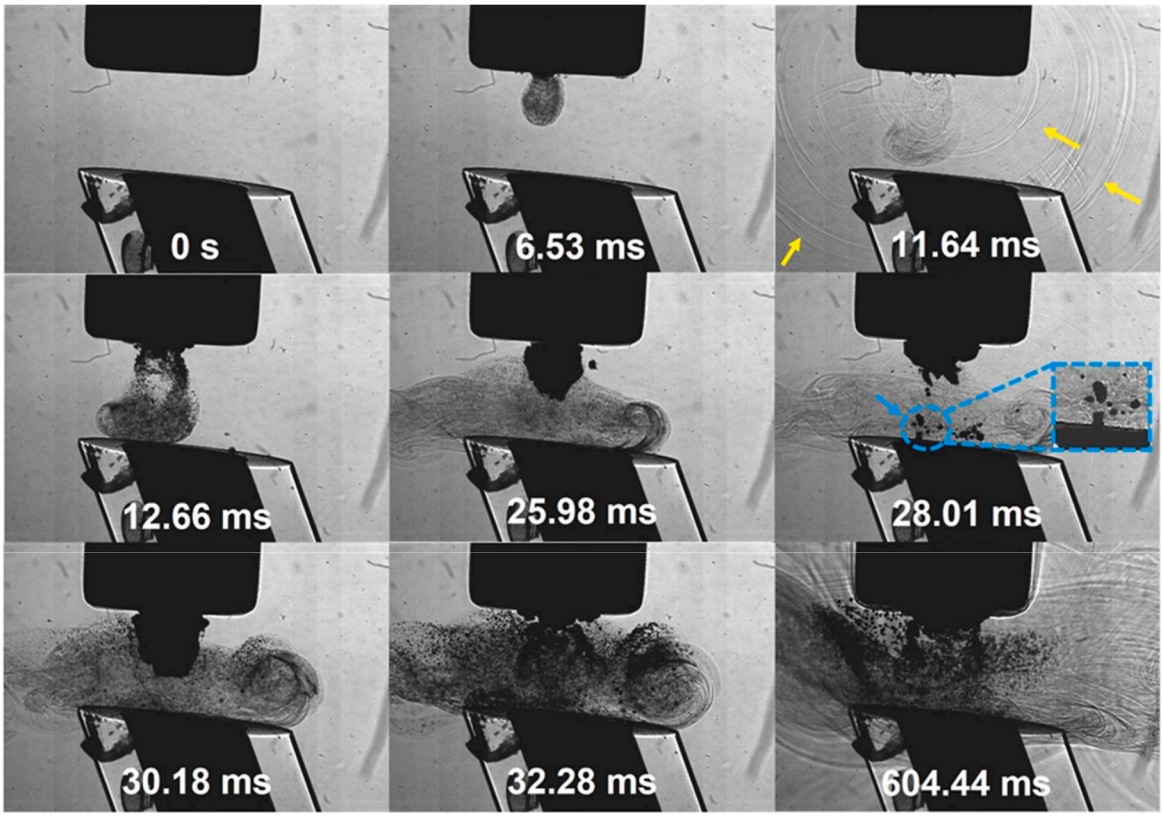

Fig. 5. High-speed imaging sequence of cavitation onset and development at electrode surface. Bubble collapse shockwaves are arrowed yellow and jetting bubbles on electrode surface arrowed blue. Full image sequence available in movie format as supplementary material. Scale provided by the 6 mm Ø ultrasonic horn tip.

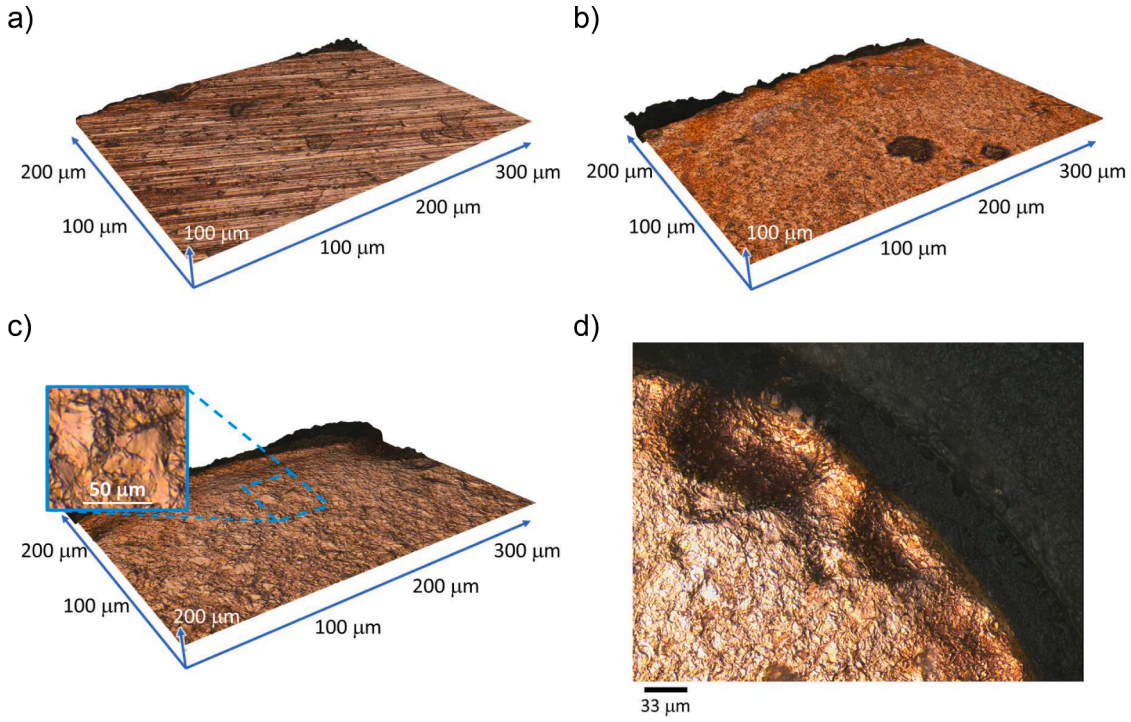

Fig. 6. a) 50 x optical profilometry of electrode surface prior to experimentations, b) 50 x optical profilometry of electrode surface after silent LSV, and c) 50 x optical profilometry after sonication at 132 W.cm^{-2} during the LSV. Insert: 2D image of the surface showing the asymmetric etching. d) HDR-2D image of surface at 50 x optical magnification showing bulk copper removal from insonated electrode. All LSV curves recorded at 10 mV.s^{-1} between −0.2 and 1.4 V (vs copper wire) in ChCl:2EG.

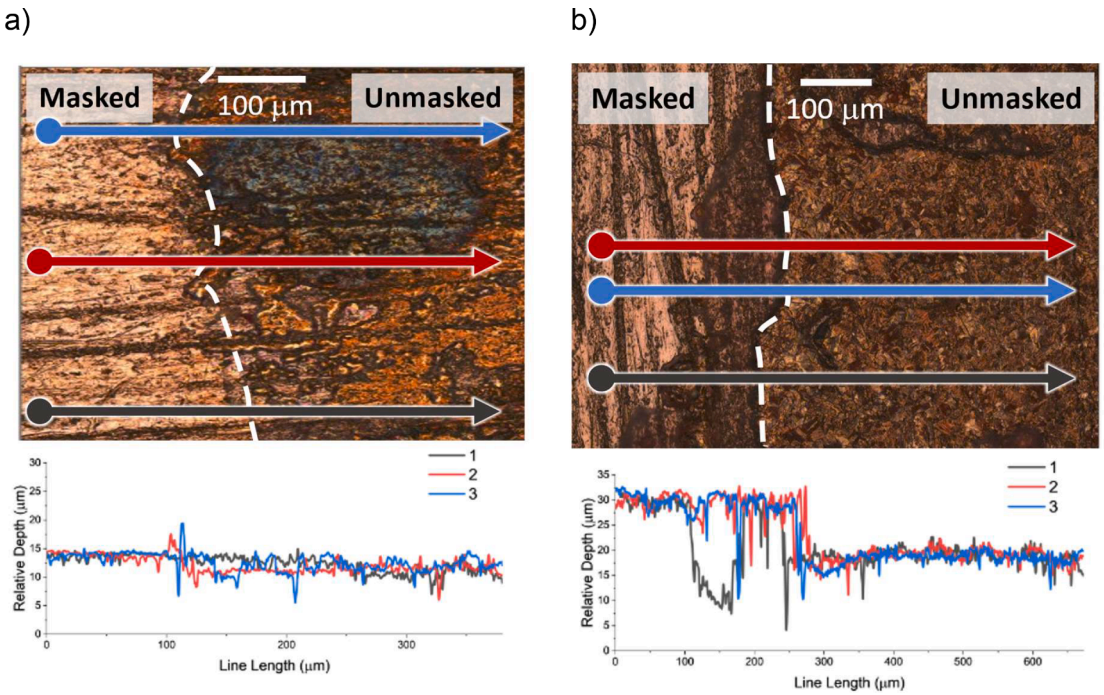

Fig. 7. Top: Copper plates after chronoamperometry (180 seconds, +1 V vs copper wire reference. a) Silent conditions, b) insonated conditions – 132 W.cm^{-2}.) 2D images recorded on Zeta Optical Profiler along the boundary between masked and unmasked areas. Dashed line included along the boundary layer added as a guide for the reader. Below: Relative heights across the pieces along the indicated lines.

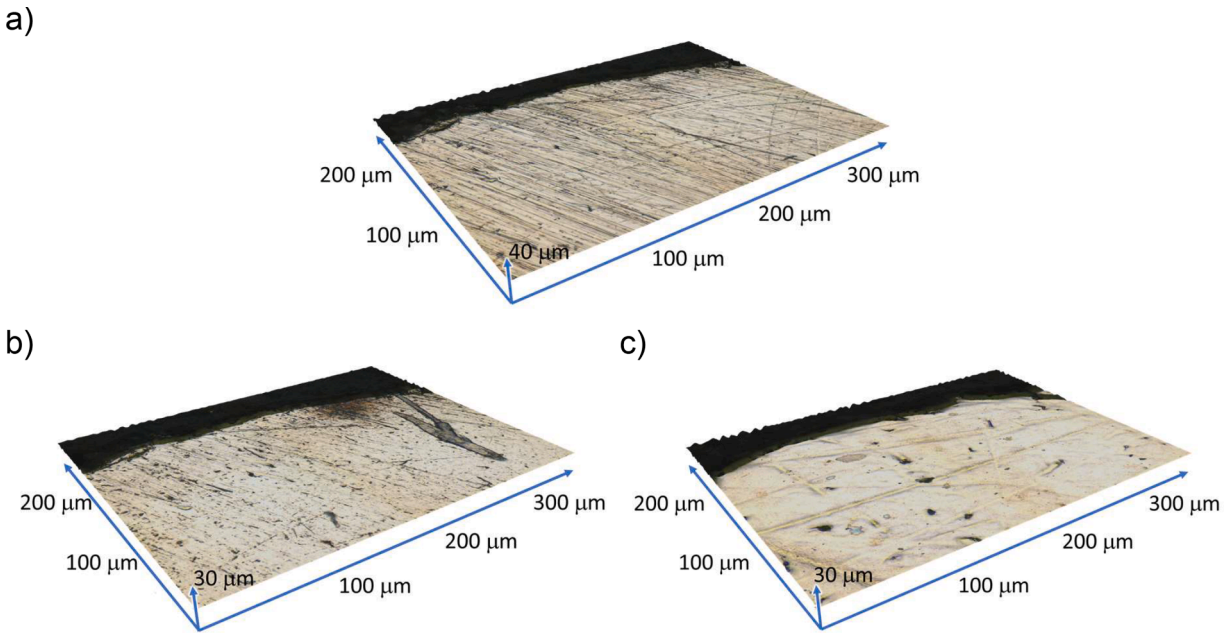

Fig. 8. a) 50 x optical profilometry of electrode surface prior to experimentations, b) 50 x optical profilometry of nickel electrode surface after silent LSV and c) 50 x optical profilometry after sonication at 132 W.cm^{-2} during the LSV. All LSV curves recorded at 10 mV.s^{-1} between −0.2 and 1.4 V (vs nickel wire electrode) in ChCl:2EG.

reference for 180 s), nickel is able to dissolve at an etch rate of 0.9 µm. min^{-1} under ultrasonic conditions, compared to effectively no etching under silent conditions (Fig. 9). There is some evidence of pitting occurring on a nickel surface under ultrasonic control, which could have been brought about by cavitation disturbing the double layer in localised areas. This shows that ultrasound is able to prevent passivation in a system where extensive passivation is observed under silent conditions.

4. Conclusions

The ultrasonically assisted electrodissolution of copper and nickel in ChCl:2EG has been investigated using linear sweep voltammetry, chronoamperometry and high-speed imaging techniques. Under silent conditions in ChCl:2EG, both copper and nickel metal LSV curves indicate the formation of a passivating layer, causing a significant decrease in current density and mass transport rate. When ultrasound is applied,

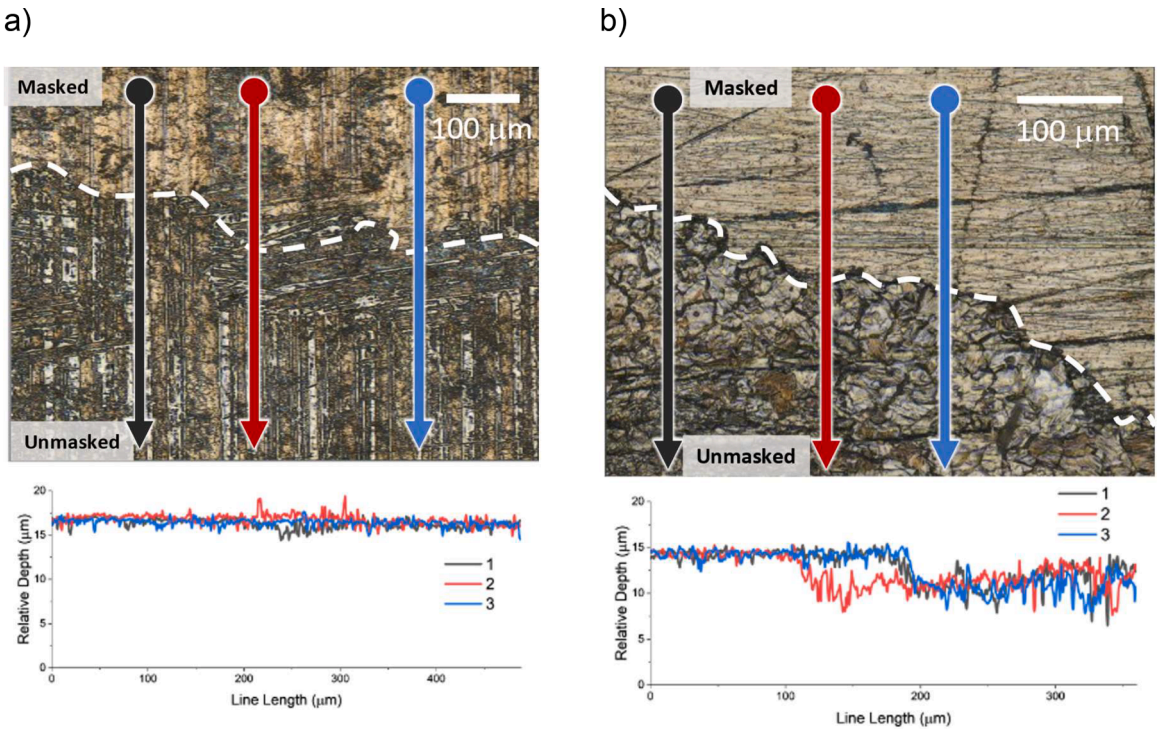

Fig. 9. Top: Nickel plates after chronoamperometry (180 seconds, +1 V vs nickel wire reference. a) Silent conditions, b) insonated conditions – 132 W.cm^{-2}.) 2D images recorded on Zeta Optical Profiler along the boundary between masked and unmasked areas. Dashed line included along the boundary layer added as a guide for the reader. Below: Relative heights across the pieces along the indicated lines.

there is no indication of passivation of the surface. The current density for the copper LSV curve has increased by a factor of 14 times at an over potential of +1.4 V (vs copper wire reference). For nickel at a + 1.4 V over potential compared to silent conditions (vs a nickel wire reference) there is 30 times increase in current density. The application of ultrasound increases mass transport of normally passivating species away from the active surface, with the current-voltage response remaining approximately linear. As the potential sweep rate is increased under ultrasonic conditions, the current density decreases, an effect of increasing the localised conductivity of the solution as metal ions are dissolved in the solution. The near linear current–potential response under ultrasonic conditions, alongside the correlation with solution conductivity is showing a migration-controlled response over a diffusion-controlled response. Further evidence of this comes from the chronoamperometric experiments, where a diffusion response would show as a decrease in current as time increases, however for both copper and nickel, the current density increases. The application of ultrasound to the surface increases both migration of species around the surface as well as increasing the surface area. High speed imaging studies have shown the bubble cloud colliding with the surface of the electrode and causing turbulent flow and mixing of the solution around the electrode surface. On top of this, asymmetric bubble collapse can be seen causing high powered jets to hit the surface, causing both large pitting seen on the copper surface and the at least partial erosion of the nickel passivation layer resulting in an earlier onset potential under insonated conditions.

CRediT authorship contribution statement

Christopher E. Elgar: Formal analysis, Investigation, Supervision, Visualization, Writing – original draft, Writing – review & editing. **Sam Ravenhill:** Investigation. **Philip Hunt:** Formal analysis, Investigation, Writing – original draft, Writing – review & editing. **Ben Jacobson:** Formal analysis, Investigation, Writing – original draft, Writing – review & editing. **Andrew Feeney:** Funding acquisition, Supervision, Writing – original draft, Writing – review & editing. **Paul Prentice:** Funding acquisition, Supervision, Writing – original draft, Writing – review & editing. **Karl S. Ryder:** Supervision, Funding acquisition, Writing – review & editing. **Andrew P. Abbott:** Conceptualization, Funding acquisition, Supervision, Writing – original draft, Writing – review & editing.

Declaration of Competing Interest

The authors declare that they have no known competing financial interests or personal relationships that could have appeared to influence the work reported in this paper.

Data availability

Data will be made available on request.

Acknowledgements

The authors would like to thank the Engineering and Physical Sciences Research Council (EPSRC) Sonocat project (EP/W018632/1), the EPSRC funded Future of Ultrasonic Engineering CDT (grant EP/S023879/1), the Natural Environment Research Council (NERC) CENTA2 research grant (NE/S007350/1), and the UKRI Interdisciplinary Circular Economy Centre for Technology Metals, Met4Tech project (EP/V011855/1) for funding this work.

Supplementary materials

Supplementary material associated with this article can be found, in the online version, at doi:10.1016/j.electacta.2023.143707.

References

[1] F. Yang, H. Kang, Z. Chen, E. Guo, Y. Zeng, W. Wang, T. Wang, Electrochemical corrosion mechanisms of nickel-aluminium bronze with different nickel contents using the rotating disc electrode, Corros. Sci. 157 (2019) 438–449, https://doi.org/10.1016/j.corsci.2019.06.018.

[2] C. Deslouis, B. Tribollet, M. Duprat, F. Moran, Transient mass transfer at a coated rotating disk electrode: diffusion and electrohydrodynamical impedances, J. Electrochem. Soc. 134 (1987) 2496, https://doi.org/10.1149/1.2100229.

[3] F.B. Leitz, L. Marinčić, Enhanced mass transfer in electrochemical cells using turbulence promoters, J. Appl. Electrochem. 7 (1977) 473–484, https://doi.org/10.1007/BF00616758.

[4] A. Speidel, J. Mitchell-Smith, I. Bisterov, A.T. Clare, The importance of microstructure in electrochemical jet processing, J. Mater. Process. Technol. 262 (2018) 459–470, https://doi.org/10.1016/j.jmatprotec.2018.07.022.

[5] J. Mitchell-Smith, A. Speidel, A.T. Clare, Advancing electrochemical jet methods through manipulation of the angle of address, J. Mater. Process. Technol. 255 (2018) 364–372, https://doi.org/10.1016/j.jmatprotec.2017.12.026.

[6] J. Klima, Application of ultrasound in electrochemistry. An overview of mechanisms and design of experimental arrangement, Ultrasonics 51 (2011) 202–209, https://doi.org/10.1016/j.ultras.2010.08.004.

[7] R.G. Compton, J.C. Eklund, F. Marken, T.O. Rebbitt, R.P. Akkermans, D.N. Waller, Dual activation: coupling ultrasound to electrochemistry—An overview, Electrochim. Acta 42 (1997) 2919–2927, https://doi.org/10.1016/S0013-4686(97)00113-8.

[8] J. Xiong, Y. Liu, C. Li, Y. Zhou, F. Li, Quantitative evaluation of the microjet velocity and cavitation erosion on a copper plate produced by a spherical cavity focused transducer at the high hydrostatic pressure, Ultrason. Sonochem. 82 (2022) 105899, https://doi.org/10.1016/j.ultsonch.2021.105899.

[9] R.G. Compton, J.C. Eklund, S.D. Page, T.J. Mason, D.J. Walton, Voltammetry in the presence of ultrasound: mass transport effects, J. Appl. Electrochem. 26 (1996) 775–784, https://doi.org/10.1007/BF00683739.

[10] F. Marken, J.C. Eklund, R.G. Compton, Voltammetry in the presence of ultrasound: can ultrasound modify heterogeneous electron transfer kinetics? J. Electroanal. Chem. 395 (1995) 335–339, https://doi.org/10.1016/0022-0728(95)04268-S.

[11] R. Ramachandran, R. Saraswathi, Sonoelectrochemical studies on mass transport in some standard redox systems, Russ. J. Electrochem. 47 (2011) 15–25, https://doi.org/10.1134/S1023193511010149.

[12] M.E. Hyde, R.G. Compton, How ultrasound influences the electrodeposition of metals, J. Electroanal. Chem. 531 (2002) 19–24, https://doi.org/10.1016/S0022-0728(02)01016-1.

[13] A.P. Abbott, Deep eutectic solvents and their application in electrochemistry, Curr. Opin. Green Sustain. Chem. 36 (2022) 100649, https://doi.org/10.1016/j.cogsc.2022.100649.

[14] J.M. Hartley, S. Scott, R.M. Rivera, P. Hunt, A.J. Lucio, P. Bird, R. Harris, G.R. T. Jenkin, A.P. Abbott, Tailoring lixiviant properties to optimise selectivity in E-waste recycling, RSC Sustain 1 (2023) 107–116, https://doi.org/10.1039/D2SU00038E.

[15] A.P. Abbott, G. Frisch, J. Hartley, W.O. Karim, K.S. Ryder, Anodic dissolution of metals in ionic liquids, Prog. Nat. Sci. Mater. Int. 25 (2015) 595–602, https://doi.org/10.1016/j.pnsc.2015.11.005.

[16] B.G. Pollet, J.Y. Hihn, T.J. Mason, Sono-electrodeposition (20 and 850kHz) of copper in aqueous and deep eutectic solvents, Electrochim. Acta 53 (2008) 4248–4256, https://doi.org/10.1016/j.electacta.2007.12.059.

[17] C.A. Schneider, W.S. Rasband, K.W. Eliceiri, NIH Image to ImageJ: 25 years of image analysis, Nat. Methods. 9 (2012) 671–675, https://doi.org/10.1038/nmeth.2089.

[18] J.H. Song, A. Moldovan, P. Prentice, Non-linear acoustic emissions from therapeutically driven contrast agent microbubbles, Ultrasound Med. Biol. 45 (2019) 2188–2204, https://doi.org/10.1016/j.ultrasmedbio.2019.04.005.

[19] N. Kudo, A simple technique for visualizing ultrasound fields without schlieren optics, Ultrasound Med. Biol. 41 (2015) 2071–2081, https://doi.org/10.1016/j.ultrasmedbio.2015.03.004.

[20] J.M. Hartley, C.M. Ip, G.C.H. Forrest, K. Singh, S.J. Gurman, K.S. Ryder, A. P. Abbott, G. Frisch, EXAFS Study into the speciation of metal salts dissolved in ionic liquids and deep eutectic solvents, Inorg. Chem. 53 (2014) 6280–6288, https://doi.org/10.1021/ic500824r.

[21] Y. Jia, A. Bi, A. Selimovic, R.S. Martin, I.Z. Kiss, Periodic and complex waveform current oscillations of copper electrodissolution in phosphoric acid in an epoxy-based microchip flow cell, J. Solid State Electrochem. 19 (2015) 3241–3251, https://doi.org/10.1007/s10008-015-2801-3.

[22] G. Zante, C.E. Elgar, K. George, A.P. Abbott, J.M. Hartley, Concentrated ionic fluids: is there a difference between chloride-based brines and deep eutectic solvents? Angew. Chem. Int. Ed. 62 (2023) e202311140 https://doi.org/10.1002/anie.202311140.

[23] A.P. Abbott, G. Frisch, H. Garrett, J. Hartley, Ionic liquids form ideal solutions, Chem. Commun. 47 (2011) 11876–11878, https://doi.org/10.1039/C1CC14801J.

[24] R.G. Compton, J.C. Eklund, F. Marken, Sonoelectrochemical processes: a review, Electroanalysis 9 (1997) 509–522, https://doi.org/10.1002/elan.1140090702.

[25] P.R. Birkin, H.M. Hirsimäki, J.G. Frey, T.G. Leighton, Mass transfer enhancement produced by laser induced cavitation, Electrochem. Commun. 8 (2006) 1603–1609, https://doi.org/10.1016/j.elecom.2006.07.026.

[26] J. Klíma, C. Bernard, C. Degrand, Sonoelectrochemistry: effects of ultrasound on voltammetric measurements at a solid electrode, J. Electroanal. Chem. 367 (1994) 297–300, https://doi.org/10.1016/0022-0728(93)03294-Y.

[27] E. Maisonhaute, C. Prado, P.C. White, R.G. Compton, Surface acoustic cavitation understood via nanosecond electrochemistry. Part III: shear stress in ultrasonic cleaning, Ultrason. Sonochem. 9 (2002) 297–303, https://doi.org/10.1016/S1350-4177(02)00089-5.

[28] P.R. Birkin, R. O'Connor, C. Rapple, S.S. Martinez, Electrochemical measurement of erosion from individual cavitation events generated from continuous ultrasound, J. Chem. Soc. Faraday Trans. 94 (1998) 3365–3371, https://doi.org/10.1039/A805934I.

[29] J. Jordens, B. Bamps, B. Gielen, L. Braeken, T. Van Gerven, The effects of ultrasound on micromixing, Ultrason. Sonochem. 32 (2016) 68–78, https://doi.org/10.1016/j.ultsonch.2016.02.020.

[30] M. Lamminen, Mechanisms and factors influencing the ultrasonic cleaning of particle-fouled ceramic membranes, J. Membr. Sci. 237 (2004) 213–223, https://doi.org/10.1016/j.memsci.2004.02.031.

[31] M.L. Doche, A. Mandroyan, M. Mourad-Mahmoud, V. Moutarlier, J.Y. Hihn, An ultrasonic-assisted process for copper recovery in a des solvent: leaching and re-deposition, Chem. Eng. Process. Process Intensif. 121 (2017) 90–96, https://doi.org/10.1016/j.cep.2017.08.006.

[32] J.A. Morton, M. Khavari, L. Qin, B.M. Maciejewska, A.V. Tyurnina, N. Grobert, D. G. Eskin, J. Mi, K. Porfyrakis, P. Prentice, I. Tzanakis, New insights into sono-exfoliation mechanisms of graphite: in situ high-speed imaging studies and acoustic measurements, Mater. Today. 49 (2021) 10–22, https://doi.org/10.1016/j.mattod.2021.05.005.

[33] S. Cleve, C. Inserra, P. Prentice, Contrast agent microbubble jetting during initial interaction with 200-kHz focused ultrasound, Ultrasound Med. Biol. 45 (2019) 3075–3080, https://doi.org/10.1016/j.ultrasmedbio.2019.08.005.

[34] R.M. Santos, D. François, G. Mertens, J. Elsen, T. Van Gerven, Ultrasound-intensified mineral carbonation, Appl. Therm. Eng. 57 (2013) 154–163, https://doi.org/10.1016/j.applthermaleng.2012.03.035.

[35] R.M. Wagterveld, L. Boels, M.J. Mayer, G.J. Witkamp, Visualization of acoustic cavitation effects on suspended calcite crystals, Ultrason. Sonochem. 18 (2011) 216–225, https://doi.org/10.1016/j.ultsonch.2010.05.006.

[36] B. Jacobson, S. Li, R.Marin Rivera, P. Daly, C.E. Elgar, D.M. Mulvihill, A.P. Abbott, A. Feeney, P. Prentice, A mechanistic study identifying improved technology critical metal delamination from printed circuit boards at lower power sonications in a deep eutectic solvent, Ultrason. Sonochem. 101 (2023) 106701, https://doi.org/10.1016/j.ultsonch.2023.106701.

[37] W.O. Karim, A.P. Abbott, S. Cihangir, K.S. Ryder, Electropolishing of nickel and cobalt in deep eutectic solvents, Trans. IMF. 96 (2018) 200–205, https://doi.org/10.1080/00202967.2018.1470400.